Core–Shell Strategy Leading to High Reversible Hydrogen Storage Capacity for $NaBH_4$

Meganne L. Christian and Kondo-François Aguey-Zinsou*

Merlin Group, ARC Center for Functional Nanomaterials, School of Chemical Engineering, The University of New South Wales, Sydney NSW 2052, Australia

ABSTRACT

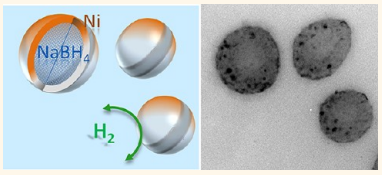

Owing to its high storage capacity (10.8 mass %), sodium borohydride ($NaBH_4$) is a promising hydrogen storage material. However, the temperature for hydrogen release is high (>500 °C), and reversibility of the release is unachievable under reasonable conditions. Herein, we demonstrate the potential of a novel strategy leading to high and stable hydrogen absorption/desorption cycling for $NaBH_4$ under mild pressure conditions (4 MPa). By an antisolvent precipitation method, the size of $NaBH_4$ particles was restricted to a few nanometers (<30 nm), resulting in a decrease of the melting point and an initial release of hydrogen at 400 °C. Further encapsulation of these nanoparticles upon reaction of nickel chloride at their surface allowed the synthesis of a core–shell nanostructure, $NaBH_4$@Ni, and this provided a route for (a) the effective nanoconfinement of the melted $NaBH_4$ core and its dehydrogenation products, and (b) reversibility and fast kinetics owing to short diffusion lengths, the unstable nature of nickel borohydride, and possible modification of reaction paths. Hence at 350 °C, a reversible and steady hydrogen capacity of 5 mass % was achieved for $NaBH_4$@Ni; 80% of the hydrogen could be desorbed or absorbed in less than 60 min, and full capacity was reached within 5 h. To the best of our knowledge, this is the first time that such performances have been achieved with $NaBH_4$. This demonstrates the potential of the strategy in leading to major advancements in the design of effective hydrogen storage materials from pristine borohydrides.

KEYWORDS: sodium borohydride · $NaBH_4$ · nickel · nanoparticle · core–shell · hydrogen storage · reversibility

With a high chemical energy density and zero emissions when produced from renewable resources, hydrogen is set to become a major fuel of the future, bridging the gap between intermittent renewables and rapidly depleting fossil fuels. It can be used across a wide range of applications, from portable electronics to energy distribution systems within the grid and transportation. The single largest challenge remaining in its implementation is storage. For on-board applications, in particular, the storage medium must be light, safe, compact, and affordable.

Hydrogen may be stored as a gas, a liquid, or bonded within a solid material. The latter is the safest approach and has a relatively high volumetric capacity. Ideally, the system should also have a hydrogen gravimetric capacity >6 mass % and low thermodynamic stability leading to hydrogen desorption near room temperature and under moderate pressures, fast kinetics for both hydrogen release and uptake, and a long cycle life (>1000 cycles).[1] At present, there is no material that satisfies all of these criteria. In materials where hydrogen is physisorbed to surfaces such as carbon, the bond strength is too weak, and cryogenic temperatures are required to achieve a useful capacity.[2] In materials where hydrogen is chemisorbed, such as in unmodified hydrides of light metals like lithium, magnesium, and sodium, the bond strength is such that very high temperatures are required for hydrogen release.[3,4]

Complex hydrides such as light metal borohydrides have very high gravimetric capacities and tend to release hydrogen at temperatures lower than their hydride counterparts.[5–7] However, desorption often occurs in multiple steps, and the temperatures required are still too high for practical applications. In addition, kinetics are slow owing to the limitations inherent to the diffusion of elements in the solid state,[8] and reversibility is impossible to achieve unless very high pressures and temperatures are used.[9–11] There has been much research into improving the thermodynamics and kinetics of these otherwise promising materials,[5,12,13] primarily focusing on destabilization by $H^{\delta+}/H^{\delta-}$ coupling,[14,15] partial cation substitution,[16] or direct reaction with another hydride[17–20] with the additional use of catalysts.[20–22] While these methods have led to some thermodynamic

* Address correspondence to f.aguey@unsw.edu.au.

Received for review April 17, 2012 and accepted August 8, 2012.

Published online August 08, 2012
10.1021/nn3030018

improvements, unfortunately they have achieved little progress toward providing a practical solution.

An alternative is a nanoscaling approach.[3,23] By restricting the size of hydride particles to a few nanometers and organizing the atoms into adequate nanostructures, both kinetics and thermodynamics could be cleverly and effectively altered.[3] Shortening ionic diffusion distances and limiting phase segregation would allow significant activation energy barriers to be overcome, and the excess of surface energy occurring in small particles would facilitate destabilization.[3,24] The potential of the approach has now been demonstrated.[25−28] However, progress in synthesizing nanosized complex hydrides remains slow because of the inherent difficulty in stabilizing such reactive materials at the nanoscale. Therefore, most efforts have focused on a nanoconfiment approach whereby the hydride is infiltrated by impregnation or melting within the nanoporosity of carbon. Hence, upon infiltration of $LiAlH_4$,[29] $NaAlH_4$,[29−32] $LiBH_4$,[29,33−36] $Li_3BN_2H_8$,[37] and $NaBH_4$[38,39] into or onto the mesoporosity of inorganic materials, initial results have indicated some significant shifts in materials properties (positive or negative) including lower temperatures for hydrogen desorption,[29,35] change of reaction paths,[27,40] partial reversibility,[27,39] and an increase or decrease in thermodynamic stability.[30,41] Although this approach contributes to an increase in basic knowledge, the use of a porous matrix presents several disadvantages including (a) a significant loss in gravimetric capacity, typically <1 mass % due to the mass of the hosting matrix and inability to fill all the pores; (b) slow hydrogen kinetics owing to the long diffusion ranges inherent to porous networks; and (c) a lack of control over the atomic arrangement that will dictate the final properties of the nanosized hydrides. Furthermore, porous inorganic materials including carbon bear a range of oxygen and hydroxyl surface groups.[42] Although these may provide some anchors to the nanoconfined particles, they would also lead to a partial oxidation of the confined complex hydride and thus some deterioration of the hydrogen storage properties. It is therefore necessary to develop alternative methods for the synthesis and stabilization of nanosized complex hydrides if high storage capacities and accurate tailoring of hydride properties through the nanoscaling approach are to be realized.

There has been little focus on $NaBH_4$ because it is believed to be irreversible for hydrogen storage, and most research has been conducted on its hydrolysis rather than thermolysis for hydrogen generation.[43,44] For automobile applications, the hydrolysis route has been put aside because of the nonreversibility of the process.[45] Establishing novel approaches that will lead to high reversible storage capacity is thus the cornerstone of further progress. $NaBH_4$ is a very interesting material for hydrogen storage purposes because it has a high gravimetric hydrogen capacity, it is stable in air, and appears to release hydrogen in a single step (reaction 1), with NaH and $Na_2B_{12}H_{12}$ as possible intermediates, compared to several steps for the other complex hydrides.[39,46,47]

$$NaBH_4 \rightarrow Na + B + 2H_2 \quad 10.8 \text{ mass}\% \ H_2 \qquad (1)$$

In this work, a novel route leading to high reversible hydrogen storage capacity with $NaBH_4$ is reported. Our strategy was to use a core−shell approach with the aim of achieving the synthesis and stabilization of isolated $NaBH_4$ nanoparticles.

Realizing the stabilization of discrete $NaBH_4$ nanoparticles would provide a path for high hydrogen storage capacity and the effective exploitation of any nanoscale effects. At first, the size of $NaBH_4$ particles was restricted to a few nanometers by adapting precipitation methods widely used for preparing nanosized inorganic materials.[48] A weak surfactant would act as a capping ligand stabilizing the nanoparticle of $NaBH_4$ and provide a platform for further modification of the nanoparticles. Second, to tackle problems associated with phase evolution, including melting, disproportionation, and Na evaporation during the release of hydrogen from $NaBH_4$,[39,49] the surfactant was displaced from the surface of the $NaBH_4$ nanoparticles and replaced by a more stable Ni coating. The Ni shell would contain the melted $NaBH_4$ core and its decomposition products but also provide a path for a "localized" destabilization of $NaBH_4$. With the successful implementation of this core−shell approach, drastic improvements in the hydrogen storage properties of $NaBH_4$ were obtained. The methodologies used are described and evolution of $NaBH_4$ properties at the nanoscale discussed as well as the remarkable hydrogen storage properties observed for nanosized $NaBH_4$.

RESULTS AND DISCUSSION

Synthesis of $NaBH_4$ Nanoparticles and Properties. A facile method for the preparation of nanoparticles is by antisolvent precipitation.[48] Nanoparticles of $NaBH_4$ were thus synthesized by exploiting the supersaturation of a hot solution of $NaBH_4$ as it was dropped into a cold hydrocarbon antisolvent. At a high degree of supersaturation, rapid nucleation occurred and the use of a surfactant, that is, tetrabutylammonium bromide (TBAB), limited the growth of the nanoparticles by steric repulsion and the formation of a precipitate (nano-$NaBH_4$).

As shown by scanning electron microscopy (SEM), bulk $NaBH_4$ used for the synthesis was mainly composed of microsized particles (Figure 1a and Supporting Information Figure S1). However, after dissolution and antisolvent precipitation, agglomerated nanosized particles were observed by SEM (Figure 1b and Supporting Information Figure S2). Further characterization by transmission electron microscopy (TEM) of nano-$NaBH_4$ revealed isolated spherical nanoparticles with a size between 2 and 60 nm (Figure 1d and

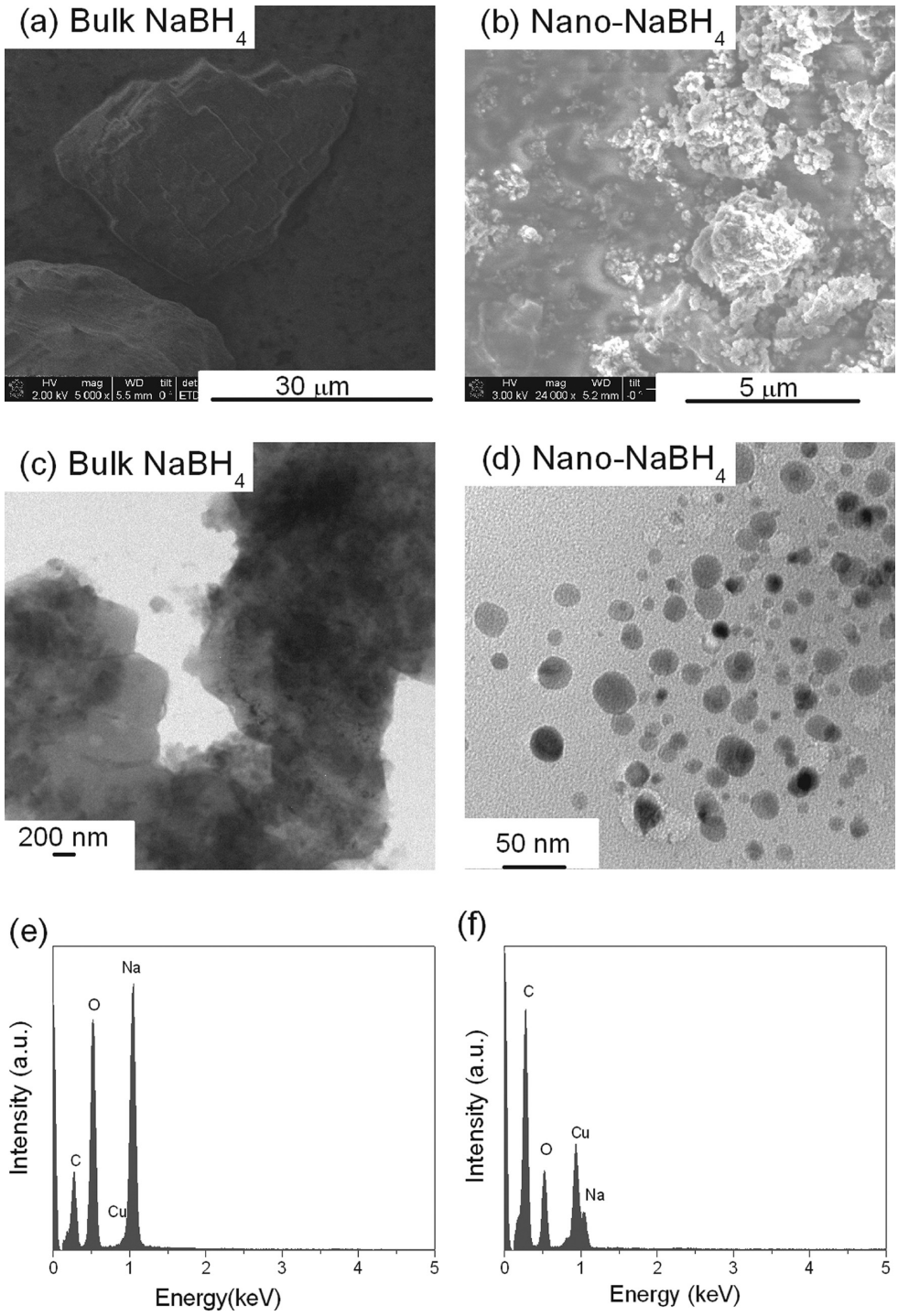

Figure 1. SEM images of (a) bulk $NaBH_4$ as-received and (b) nanoparticles as-synthesized (nano-$NaBH_4$). TEM images of (c) bulk $NaBH_4$ as-received, (d) nano-$NaBH_4$, and corresponding EDS analysis (e) for bulk $NaBH_4$ and (f) for nano-$NaBH_4$.

Supporting Information Figure S2). In comparison, only large particles with irregular shapes were observed by TEM for bulk $NaBH_4$ (Figure 1c and Supporting Information Figure S1). Furthermore, analysis by energy-dispersive X-ray spectroscopy (EDS) effectively confirmed the sodium content of nanoparticles observed (Figure 1e,f), and characterization by X-ray diffraction (XRD) proved that these nanoparticles corresponded to the cubic structure of crystalline $NaBH_4$, that is, the α-$NaBH_4$ phase (Figure 2). It is noteworthy that there was no change in crystalline phase upon $NaBH_4$ precipitation as compared to bulk $NaBH_4$. The diffraction pattern of nano-$NaBH_4$ also displayed peaks below $2\theta = 30°$, and these were attributed to the excess of surfactant recrystallizing upon drying. Furthermore, Scherrer analysis of the diffraction pattern of nano-$NaBH_4$ gave an average crystallite size of 13 nm, a value somewhat smaller than that of bulk $NaBH_4$ (*i.e.*, 41 nm,

Table 1). Hence, most of the particles observed by TEM would be single $NaBH_4$ crystals.

To compare the hydrogen desorption properties of the nanoparticles with that of the bulk $NaBH_4$, each was subjected to a heating ramp and simultaneous monitoring of heat flow, weight loss, and hydrogen release. By differential scanning calorimetry (DSC), two main endothermic events were observed at 500 and 550 °C for bulk $NaBH_4$ (Figure 3a). The first one was attributed to the melting of $NaBH_4$ and the second to its decomposition in agreement with previous reports.[47,49,50] Indeed, hydrogen was detected between 500 and 600 °C by mass spectrometry (MS), and a single decomposition step was simultaneously observed by thermogravimetric analysis (TGA). Furthermore, the mass loss observed by TGA was much higher than the theoretical 10.8 mass % of hydrogen in $NaBH_4$. This would indicate a substantial evaporation of sodium (~17 mass %) during the course of $NaBH_4$ decomposition, in agreement with previous investigations.[39] Since sodium is melting at 97.8 °C and has a high vapor pressure at 500 °C,[51] some evaporation can be expected during TGA measurement.

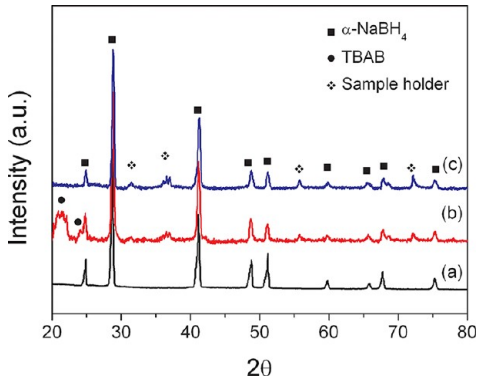

Figure 2. XRD patterns of (a) bulk $NaBH_4$ as-received, (b) nano-$NaBH_4$ as-synthesized, and (c) nano-$NaBH_4$ after heating under static vacuum (0.01 MPa) at 400 °C for 5 h.

TABLE 1. Particle and Crystallite Sizes of $NaBH_4$ As-Received, Nano-$NaBH_4$, and $NaBH_4$@Ni

	particle size by TEM (nm)	crystallite size from Scherrer equation (±5 nm)
$NaBH_4$ as-received		41
nano-$NaBH_4$	2—60	13
$NaBH_4$@Ni	10—200	16

For nano-$NaBH_4$, a similar decomposition behavior was observed, although an additional endothermic peak at 100 °C was detected and the two endothermic peaks corresponding to the melting and/or decomposition of $NaBH_4$ were found at temperatures of 460 and 535 °C, respectively (Figure 3b). The first endothermic peak at 100 °C and associated decomposition step at 200 °C were attributed to the melting and decomposition of TBAB, as masses corresponding to the thermal degradation of TBAB were detected by MS in this temperature range (Figure 3b and Supporting Information Figure S3). It is noteworthy that the temperature of TBAB decomposition in nano-$NaBH_4$ is close to that of pristine TBAB (Supporting Information Figure S3), indicating a weak surfactant/$NaBH_4$ interaction unable to prevent any potential melting of the $NaBH_4$ nanoparticles and subsequent agglomeration and sintering. TEM analysis further confirmed the tendency of the "naked" $NaBH_4$ nanoparticles to agglomerate and

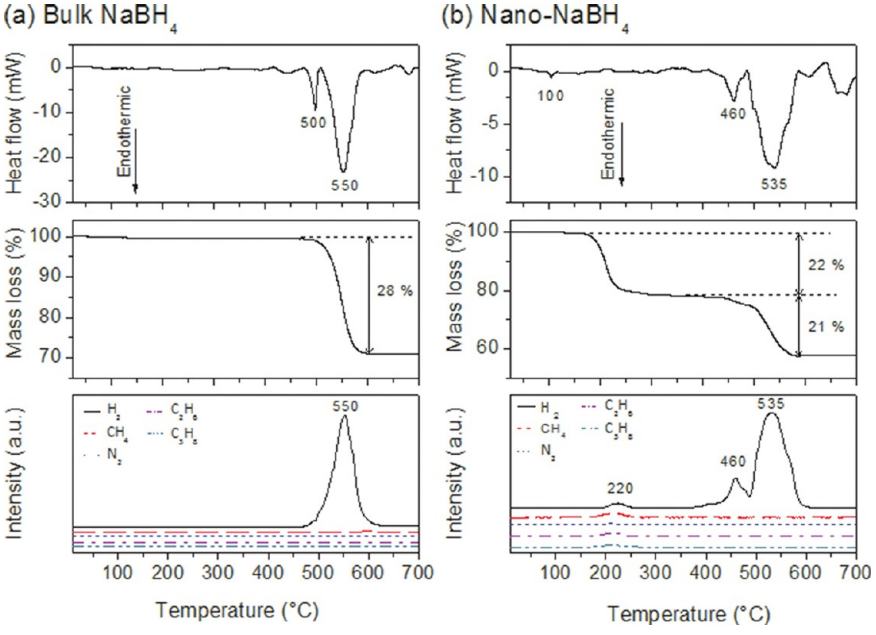

Figure 3. Thermal decomposition of (a) $NaBH_4$ as-received and (b) nano-$NaBH_4$ as-synthesized, characterized by TGA/DSC/MS analysis. No other gases were detected by MS.

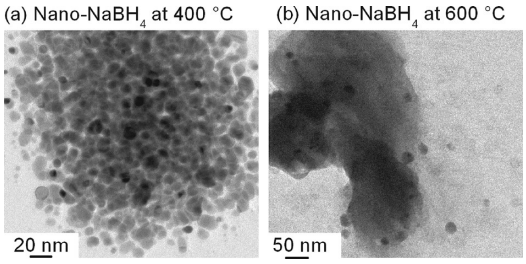

Figure 4. TEM images of nano-$NaBH_4$ after heating the material up to (a) 400 °C and (b) 600 °C. Heating was performed by TGA under a temperature ramp of 10 °C·min^{-1} and an Ar flow of 25 mL·min^{-1}.

sinter as the temperature was increased above 400 °C and large aggregates with only a few isolated nanoparticles were found at 600 °C (Figure 4 and Supporting Information Figure S4). Further XRD analysis confirmed that any hydrogen desorption observed below 400 °C for nano-$NaBH_4$ was due only to the decomposition of TBAB (Figure 2). Despite the low particle sizes of nano-$NaBH_4$ (*i.e.*, 2−60 nm), hydrogen desorption started at temperatures above 400 °C in two successive events peaking at 460 and 535 °C. The onset temperature for hydrogen release from nano-$NaBH_4$ was still lower compared to that of bulk $NaBH_4$ (380 °C instead of 475 °C, Figure 3), and this may indicate that an adequate stabilization of $NaBH_4$ nanoparticles could lead to lower temperatures for hydrogen release. Indeed, $NaBH_4$ nanoconfined in porous carbon has been reported to release hydrogen from 150 °C with a peak at 350 °C,[38,39] and this may be due to an effective confinement of $NaBH_4$. It is difficult from the DSC result to determine whether the nanoparticles of $NaBH_4$ melted before decomposition because all of the endothermic peaks observed were accompanied by a release of hydrogen (Figure 3b). It is possible that the nanoparticles melted with simultaneous release of hydrogen due to the short diffusion lengths involved in small particles. Overall, a 22% mass loss related to the decomposition of TBAB was first observed by TGA up to 350 °C (Figure 3b), and this would correspond to a hydrogen content of 8 mass % in nano-$NaBH_4$. However, at temperatures above 350 °C during hydrogen release, a 21% mass loss was recorded (Figure 3b). Once again, this excessive mass loss may reflect the evaporation of sodium. Accordingly, the premature decomposition of the stabilizing surfactant coupled with the evaporation of sodium would hinder any reversibility since, at the temperatures required for hydrogen desorption, the properties of nano-$NaBH_4$ would tend toward that of bulk $NaBH_4$. Indeed, attempts to cycle the nano-$NaBH_4$ were unsuccessful (Supporting Information Figure S5). Bulk $NaBH_4$ is very stable (ΔH = −108 kJ·mol^{-1} of H_2 and ΔS = 133 J·K^{-1}·mol^{-1} of H_2),[52] and to the best of our knowledge, reversibility of hydrogen desorption from bulk $NaBH_4$ has never been reported. This may be due to the need for ensuring a close vicinity of its decomposition products.[24]

A method is thus required to fully contain the decomposition products so reversibility can be achieved with high storage capacity. For this, nanoconfinement using porous carbon would not be the most effective strategy as the external opening of the nanopores would provide a path through which the melt can disperse, as evidenced by the problems of sodium evaporation encountered with $NaBH_4$ nanoconfined in porous carbon.[39] A better strategy is to encapsulate the nanoparticles within a shell that would prevent the melt from escaping while still allowing hydrogen diffusion through. An additional strength of this strategy is the opportunity for enhanced kinetics and adequate destabilization of $NaBH_4$. By using a metal forming a borohydride of lower stability than $NaBH_4$, hydrogen kinetics could be enhanced by the unstable borohydride shell "pumping" hydrogen in/out of the $NaBH_4$ core. Further thermodynamic improvements could result from the formation of intermediate bimetallic borohydrides or borides leading to an additional destabilization of the $NaBH_4$ nanoparticles. Indeed, the combination of two metallic cations of different electronegativities has been shown to lead to bimetallic borohydrides of intermediate thermodynamic stability.[12] Similarly, the stabilization of the dehydrogenation products and, in particular, boron through the formation of borides may facilitate the reversibility of the hydrogen desorption reaction since the activation energy needed to break a metal−B bond may be significantly lower than that of a B−B bond.[46,53]

Stabilization of Nano-$NaBH_4$ with a Ni Shell. Ni was chosen to coat the nanoparticles of $NaBH_4$ because it has a high melting temperature as compared to $NaBH_4$,[51] forms unstable borohydrides,[54] and has been reported to effectively catalyze the dehydrogenation/hydrogenation of $LiBH_4$ through the formation of nickel boride.[55] A simple way to coat the surface of the borohydride nanoparticles is to adapt the methods developed for the synthesis of inorganic core−shell structures and, in particular, transmetalation methods and methods involving the formation of a stable shell through a chemical reaction between the shell and the core.[56,57] In the transmetalation method, a metallic shell is formed by the reduction of a metal salt at the surface of a core initially synthesized. As the metal salt is reduced and deposited at the surface of the core, the reaction products diffuse through the shell layer into the bulk solution, leading to a homogeneous growth of the shell. On the basis of these principles, the reducing property of $NaBH_4$ could be similarly used to form $NaBH_4$@metal core−shell structures since $NaBH_4$ can readily reduce transition metal salts into their metallic counterparts. Hence, Ni could be coated at the surface of $NaBH_4$ by a sacrificial method (Scheme 1), whereby the surface of the $NaBH_4$ nanoparticles is partially consumed. In a solvent where $NaBH_4$ is not soluble, such as an organic solvent like tetrahydrofuran, this would

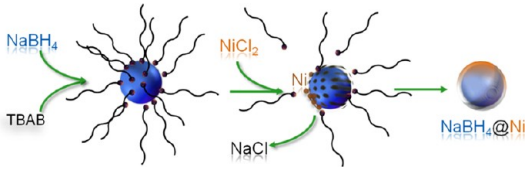

Scheme 1. Approach used for the synthesis and stabilization of $NaBH_4$ nanoparticles.

lead to the formation of a Ni shell around the $NaBH_4$ nanoparticles. For nickel chloride ($NiCl_2$), the reduction in an organic solvent would possibly lead to the formation of metallic nickel (Ni) and nickel boride (Ni_2B) following reactions 2a and 2b, with sodium chloride (NaCl) as byproduct and the evolution of hydrogen and diborane.[58]

$$2NiCl_{2(s)} + 4NaBH_{4(s)} \rightarrow 2Ni(BH_4)_{2(s)} + 4NaCl_{(s)} \quad \textbf{(2a)}$$

$$2Ni(BH_4)_{2(s)} \rightarrow \frac{1}{2}Ni_2B_{(s)} + Ni_{(s)} + \frac{7}{2}H_{2(g)} + \frac{3}{2}B_2H_{6(g)} \quad \textbf{(2b)}$$

After the reaction between nano-$NaBH_4$ (a white material) and $NiCl_2$ had taken place, the black material obtained proved the reduction of $NiCl_2$ into metallic Ni. Attempts to redissolve this material in diglyme (in which $NaBH_4$ is soluble) were unsuccessful, and this was taken as an indirect proof of the formation of a stable Ni shell around the $NaBH_4$ nanoparticles. By SEM, agglomerates of nanosized particles were once more observed, and elemental mapping by EDS revealed the close vicinity of Ni and Na, their homogeneous distribution, and thus the possible formation of a Ni shell at the surface of the $NaBH_4$ nanoparticles (Figure 5 and Supporting Information Figure S6). To confirm this, TEM analysis was carried out and isolated nanoparticles with a broad particle size distribution (10−200 nm) were imaged (Figure 6a,b and Supporting Information Figure S7). At the surface of these nanoparticles, darker particles (<2 nm) were also observed, and these would correspond to Ni nanoparticles because Ni has a higher electron density and allows fewer electrons to be transmitted. Indeed, EDS confirmed the composite nature of the nanoparticles imaged because Na and Ni were detected (Figure 6c), and XPS analysis further proved the metallic nature of the Ni composing the material (Figure 6d). This apparent contrast of the darker nanoparticles suggests a coating of the $NaBH_4$ nanoparticles with a shell composed of many small Ni particles. Furthermore, imaging of these nanoparticles at a higher magnification revealed a significant change of brightness between the center and the edges of the nanoparticles (Figure 6b, inset), and this would also be an indicator of the formation of a $NaBH_4$ core with a Ni shell because Na has a much lower electronic density than Ni. Furthermore, in dark-field TEM mode, these nanoparticles were found to be entirely bright, and this

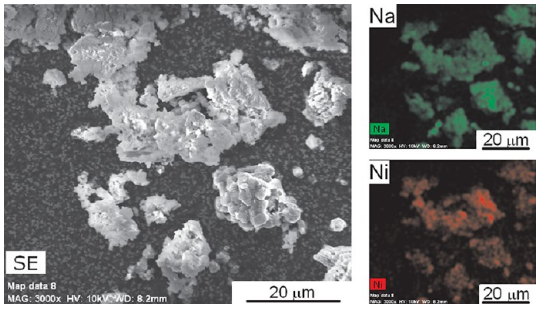

Figure 5. SEM image of $NaBH_4$@Ni and its associated EDS elemental map for Na (Kα) and Ni (Kα). What may appear as small particles in the background is due to the carbon tape.

would be another indicator of a homogeneous coating of Ni at the surface of $NaBH_4$ (Figure 6e). Additional elemental mapping by scanning transmission electron microscopy (STEM) also corroborated these conclusions with Na and Ni detected within the same particles (Figure 6f). From these observations, it was thus concluded that a core−shell structure $NaBH_4$@Ni was formed, in which $NaBH_4$ acts as the core while Ni is the shell and the thickness of this Ni shell would be <10 nm because Na and B could also been seen within the 10 nm penetration depth of the XPS instrument used (Supporting Information Figure S8).

Analysis by XRD further corroborated the formation of a core−shell structure since the intensity of the α-$NaBH_4$ phase was found to significantly decrease in intensity (Figure 7a). Indeed, with a uniform coating, a decrease in intensity of the diffraction peaks from the core should be expected.[57] By XRD, peaks related to Ni were also observed, and this further evidenced the composite nature of the material synthesized. Furthermore, since there was no phase change observed for $NaBH_4$, it is unlikely that a Ni-$NaBH_4$ alloy was formed, and thus the core−shell scenario with distinct Ni and $NaBH_4$ phases was also strongly supported by the XRD analysis. Additionally, NaCl was observed by XRD as a byproduct of the reaction of $NiCl_2$ with the $NaBH_4$ core, but no Ni_2B was detected. Nonetheless, it is possible that amorphous Ni_2B was formed according to reaction 2b. It is noteworthy that some particles in nano-$NaBH_4$ grew by around 5 times during the coating process, although the crystallite size remained constant (Table 1). One possible explanation is that during the reduction of $NiCl_2$ at the surface of the surfactant-stabilized $NaBH_4$ nanoparticles, inherent micellar collisions caused the agglomeration of several particles. Finally, no TBAB was found by XRD (Figure 7a) and Raman spectroscopy (Figure 7b) after Ni coating, and this may be an indicator that most of the surfactant has been washed away during the Ni coating process and consecutive washing. The $NaBH_4$ nanoparticles may then just be stabilized by the Ni shell.

Hydrogen Storage Properties of the Core−Shell $NaBH_4$@Ni. The thermal behavior and stability of $NaBH_4$@Ni was

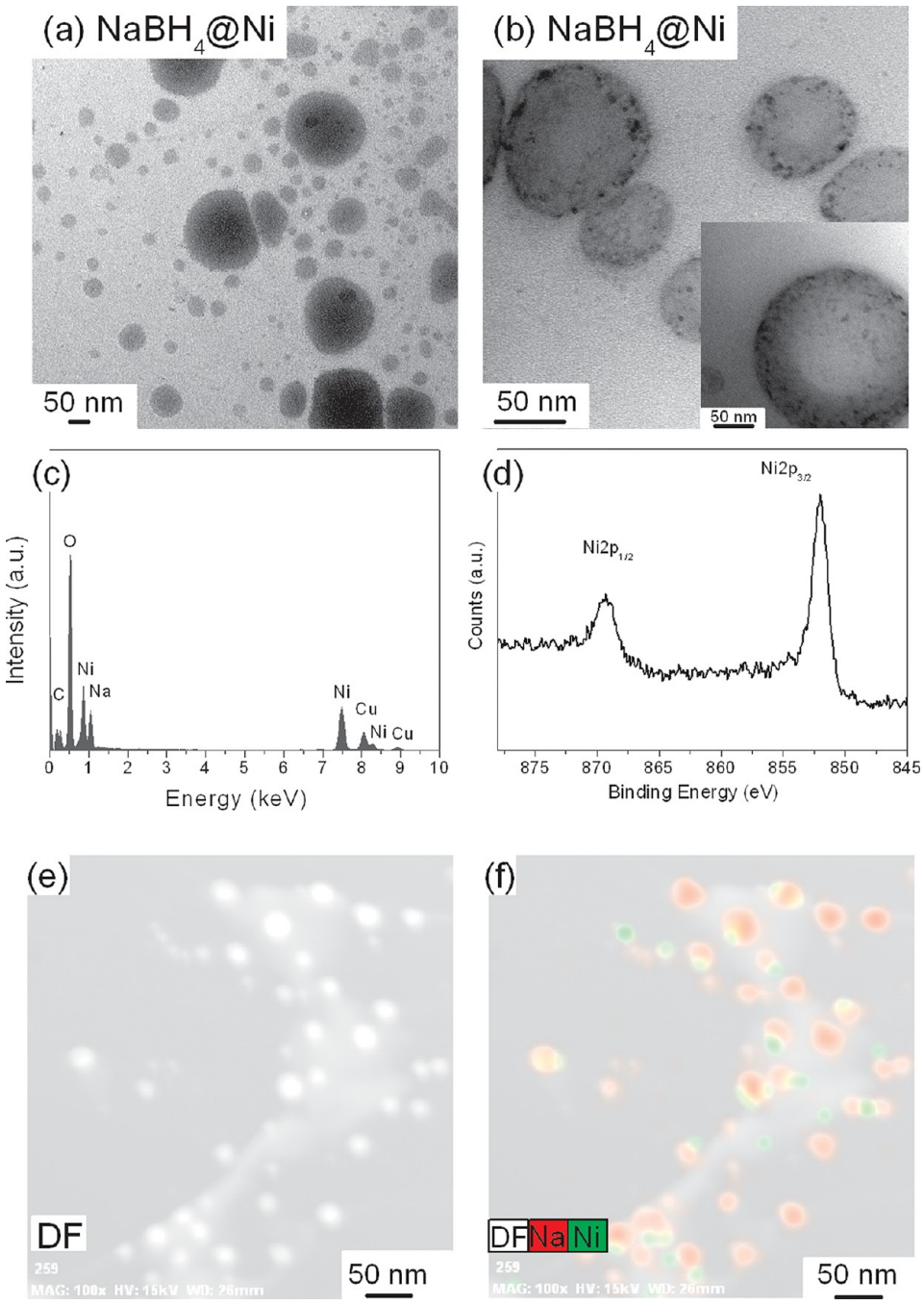

Figure 6. TEM images of (a,b) nano-$NaBH_4$ coated with Ni ($NaBH_4$@Ni) and corresponding (c) EDS analysis and (d) XPS narrow scan for Ni2p. Inset (b) $NaBH_4$@Ni at a higher magnification. The peaks at 869.3 and 852.0 eV correspond to metallic Ni.[62] STEM images of $NaBH_4$@Ni (e) in dark-field mode and (f) corresponding elemental map showing the overlap of Na (Kα) and Ni (Kα).

first investigated. Figure 8a shows the TGA/DSC for the thermal decomposition of $NaBH_4$@Ni after synthesis. Interestingly, MS showed that hydrogen began to be released at a temperature of only 50 °C, that is, 100 °C lower than that of $NaBH_4$ nanoconfined in porous carbon (Figure 8b).[38,39] Significant desorption appeared from 350 °C with an endothermic peak at 418 °C, and at 515 °C, a smaller amount of hydrogen was also released (Figure 8a,b). Importantly, no other gases than hydrogen were detected by MS throughout the decomposition process of $NaBH_4$@Ni, and this would further corroborate the initial results of XRD and Raman showing the disappearance of TBAB initially used to stabilize the $NaBH_4$ nanoparticles (Figure 7). According to the TGA curve, ~5.8 mass % of hydrogen was released through the first main endothermic event at 418 °C and the corresponding main hydrogen peak observed by MS. At temperatures above 550 °C, no further hydrogen was detected and the additional weight loss observed by TGA and associated endothermic events

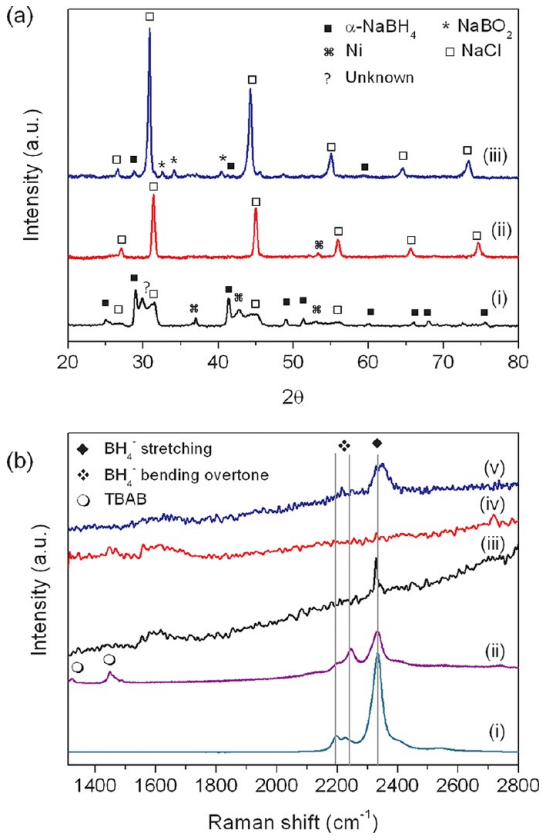

Figure 7. (a) XRD patterns of $NaBH_4$@Ni (i) as-synthesized, (ii) after hydrogen desorption at 350 °C, and (iii) after hydrogen absorption at 350 °C. (b) Raman spectra of (i) bulk $NaBH_4$ as-received, (ii) nano-$NaBH_4$ as-synthesized, (iii) $NaBH_4$@Ni as-synthesized, (iv) $NaBH_4$@Ni after hydrogen desorption at 350 °C, (v) $NaBH_4$@Ni after hydrogen absorption at 350 °C. All Raman bands could be assigned to $NaBH_4$[61,63] and TBAB.[64]

may correspond to some recrystallization and degradation of the material at very high temperatures. Indeed, further characterization of the evolution of the material morphology as a function of the temperature revealed no significant change in morphology up to 350 °C (Figure 8c and Supporting Information Figure S7). However, at 450 °C, the shape of the nanoparticles evolved from spherical to cubic, indicating a significant reconstruction and recrystallization of the material (Figure 8d and Supporting Information Figure S7). A possible explanation for such a reconstruction would be the sintering of the Ni nanoparticles at the surface of the $NaBH_4$ core since Ni nanoparticles have been shown to undergo some sintering at temperatures above 400 °C.[59,60] Nonetheless, the nanoparticles remained discrete without agglomeration, showing once more that our core–shell approach was successful in leading to stable nanostructures even at high temperatures. However, at a very high temperature of 650 °C, the structure of the particles was found to fully degrade (Figure 8e), and this would explain the additional weight loss observed by TGA at this temperature.

The temperature required to release hydrogen from $NaBH_4$@Ni is significantly lower than that of bulk or nano-$NaBH_4$ (Figure 3), and the widespread temperature range (50 to 450 °C) for hydrogen release would suggest different hydrogen bond strengths within the material or an effect of particle sizes (giving the wide particle size distribution obtained). This remarkable improvement in hydrogen desorption could be explained by a catalytic and/or destabilization effect of dispersed Ni particles within the $NaBH_4$ phase, but hydrogen desorption from Ni physically mixed with nano-$NaBH_4$ followed that of the bulk borohydride (Figure 8b). Furthermore, the large weight losses due to sodium evaporation that were seen in both bulk and nano-$NaBH_4$ could be suppressed with $NaBH_4$@Ni. Thus the improvement observed indirectly proved the formation of a core–shell structure and also the superiority of our strategic approach in leading to enhanced hydrogen desorption behavior for $NaBH_4$.

Since the $NaBH_4$@Ni nanoparticles retained their structural integrity after desorption at temperatures below 450 °C, the reversibility of hydrogen desorption was investigated. At 350 °C, a stable reversible storage capacity of 5 mass % was measured, a value close to that observed by TGA for the main hydrogen desorption at 418 °C (Figures 8a, 9a, and Supporting Information Figure S5) and also in agreement with the results from elemental analysis showing a theoretical hydrogen capacity for $NaBH_4$@Ni of 5.3 ± 1 mass %. The hydrogen kinetics were quite fast with 80% of the hydrogen desorption/absorption occurring in 60 min. However, it took 5 h to reach full storage capacity. The stability during cycling was also remarkable, with the fifth hydrogen desorption/absorption cycle almost identical to the kinetic curves of the first cycle. Further characterization by TGA/DSC/MS proved the reversibility of the reaction, and that only hydrogen was released from the material during cycling (Figure 8b and Supporting Information Figure S9). The third hydrogen desorption profile, as measured by MS, was relatively similar to the first one, although slightly broader (Figure 8b). Additional analysis by XRD of $NaBH_4$@Ni after desorption only showed peaks related to the recrystallization of the NaCl byproduct (Figure 7a). However, after hydrogen absorption, the reappearance of peaks corresponding to α-$NaBH_4$ and $NaBO_2$ proved that the material was effectively going through hydrogen desorption and absorption cycles. Due to the setup of the XRD sample holder used, potential oxidation of the material may have led to the formation of $NaBO_2$. Nonetheless, such a phase was an indirect proof of the formation of $NaBH_4$. To clarify this, Raman investigations were carried out using a capillary sealed in a glovebox under high purity Ar (O_2, H_2O <1 ppm). After hydrogen desorption, the vibration corresponding to B–H stretching at 2333 cm^{-1} disappeared and reappeared after hydrogen absorption with a broadening

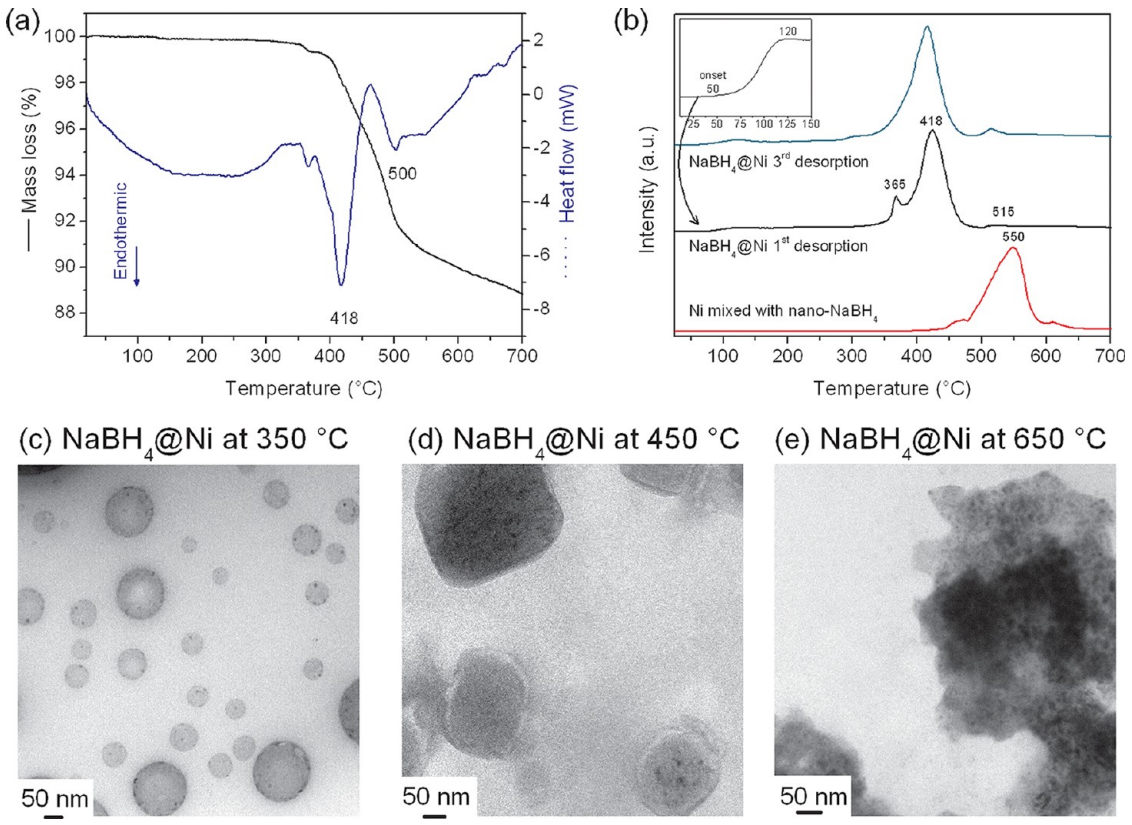

Figure 8. (a) Thermal decomposition as characterized by TGA/DSC of $NaBH_4$@Ni as-synthesized. (b) Hydrogen evolution as characterized by MS for Ni physically mixed with nano-$NaBH_4$, $NaBH_4$@Ni as-synthesized, and $NaBH_4$@Ni after undergoing 2 cycles at 350 °C. Inset magnifies the onset of hydrogen release. No other gases were detected by MS. TEM images of $NaBH_4$@Ni after heating the material up to (c) 350 °C, (d) 450 °C, (e) and 650 °C. The evolution in morphology observed was not reversible.

that could be related to a phase change and/or an increase in disorder that should be expected for small particle sizes (Figure 7b).[61] Nonetheless, this result further established the reversibility of the reaction. The morphology of $NaBH_4$@Ni was also characterized by TEM and EDS mapping after the fifth cycle (Figure 9b). It appeared that the core−shells retained their original spherical shape and core−shell structure, although darker particles were not observable at the surface of the $NaBH_4$ particles anymore. This would corroborate the hypothesis of sintering and/or potential reaction of the Ni nanoparticles at the surface of the $NaBH_4$ core. After cycling, the Ni phase was not clearly apparent in XRD (Figure 7a). Hence, Ni may have reacted with $NaBH_4$ or its decomposition products to form intermediate amorphous phases.

With a reversible storage capacity of 5 mass %, the properties of $NaBH_4$@Ni are remarkable. To the best of our knowledge, this is the first time that such a level of performance has been achieved with $NaBH_4$. In comparison, only partial reversibility was obtained with $NaBH_4$ nanoconfined in porous carbon, and the storage capacity drastically dropped from ~1 mass % to less than 0.2 mass % after the fourth hydrogen desorption.[39] Therefore, the methodologies advanced here provide a very powerful tool to control the hydrogen storage properties of borohydrides. The exact nature of such improvements are uncertain, but they could be related to several factors including the difference in electronegativity (0.98 on the Pauling scale) between Ni and Na. Good correlations have been found between the thermal stability of borohydrides and the electronegativity of their metallic cations.[12] Hence, multication borohydrides have enthalpies somewhere between those of their parent borohydrides, which could explain the improvement in hydrogen release temperature. In addition, at small particle sizes, the increase in surface area would result in a low mean coordination number of surface atoms and thus an excess of surface energy (ΔW_{surf}) that would lead to a modification of the thermodynamics and equilibrium pressure (P_{eq}) according to the following equation:[3]

$$\ln P_{eq} = \frac{1}{RT}(\Delta H^0 + \Delta W_{surf}) - \frac{\Delta S}{R} \qquad (3)$$

Such an increase in surface energy may lead to a reduction of the enthalpy (in addition to possible alloying effects at the Ni/$NaBH_4$ interface) but also additional changes in entropy that could result in an overall decrease of P_{eq}. It is noteworthy that neither B nor $Na_2B_{12}H_{12}$ was detected by Raman spectroscopy, indicating that

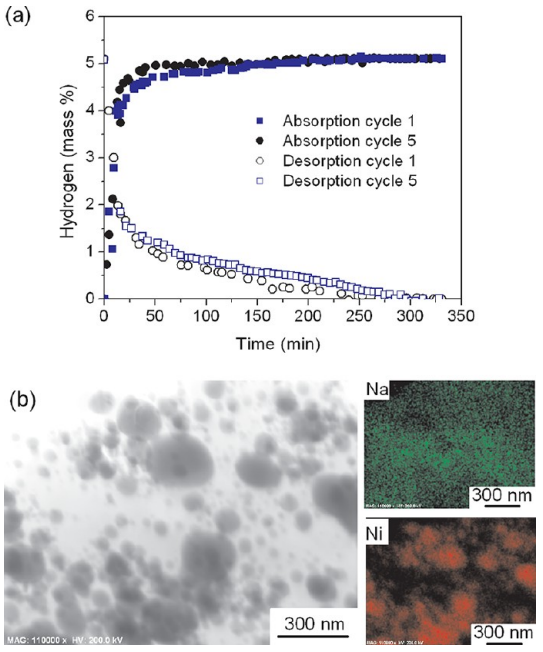

Figure 9. (a) Kinetics of hydrogen desorption at 0.01 MPa and absorption under 4 MPa hydrogen pressure at 350 °C for $NaBH_4$@Ni. Under similar conditions, nano-$NaBH_4$ physically mixed with Ni did not absorb any hydrogen. Five cycles were performed to demonstrate the stability of the hydrogen storage properties of $NaBH_4$@Ni. (b) TEM image of $NaBH_4$@Ni after 5 cycles and associated STEM elemental maps for Na (Kα) and Ni (Kα) signals. The lower resolution of the Na map is possibly due to overlaps with Ni (Lα) and X-ray interferences because of the close vicinity of the particles simultaneously excited.

the reaction path may differ from that observed for $NaBH_4$ nanoconfined in porous carbon[39] or NaH and B mixtures partially rehydrogenated.[46] In both cases, rehydrogenation was limited by the lack of reactivity of $Na_2B_{12}H_{12}$. Hence, our work clearly demonstrates that the core–shell strategy advanced here may provide alternatives to modify reaction thermodynamics and/or reaction paths. This should enable reversibility with borohydrides under practical conditions if both the enthalpy and entropy can be effectively adjusted. Optimization of the synthetic route would also allow a higher hydrogen storage capacity of ~8 mass % to be reached with the removal of the NaCl salt.

CONCLUSIONS

A novel strategy for controlling the properties of $NaBH_4$ has been demonstrated, and the effect of this strategy on the hydrogen storage properties of $NaBH_4$ has been investigated. By using precipitation methods, $NaBH_4$ nanoparticles have been successfully synthesized and stabilized with a surfactant. The onset for hydrogen desorption from these nanoparticles was reduced by around 100 °C. Further displacement of the surfactant with $NiCl_2$ led to the formation of a core–shell nanostructure, $NaBH_4$@Ni, providing a framework for solving problems associated with the melting of $NaBH_4$ and Na evaporation. Hence, with this core–shell strategy successfully in place, the release of hydrogen began from only 50 °C with significant desorption from 350 °C, and more remarkably, $NaBH_4$ became fully reversible for the first time with hydrogen desorption/absorption occurring under relatively mild conditions of pressure (4 MPa) and temperature (350 °C). Furthermore, problems of sodium evaporation encountered in previous studies were inhibited by this strategy. The storage capacity of $NaBH_4$@Ni was found to be of 5 mass % (corresponding to full desorption of the $NaBH_4$ present), and hydrogen kinetics were very fast as 4 mass % of hydrogen could be loaded/unloaded during 5 cycles in less than 60 min. Various hypotheses have been discussed to explain such remarkable improvements in kinetics and thermodynamics. These may be due to the combination of several factors including (a) small particle size effects, (b) formation of an unstable nickel borohydride shell and/or Ni destabilization, and (c) modification of reaction paths. In comparison to current nanoconfiment approaches using porous carbon or inorganic materials, our core–shell strategy provided a platform for maximizing the hydrogen storage capacity as the shell can also store hydrogen and for additional modification of the properties of $NaBH_4$ since an appropriate metallic coating would provide a means for a "localized" adjustment of the properties of $NaBH_4$. The new materials that could be generated by this exciting strategy could provide practical solutions to meet many of the targets set forward by the U.S. Department of Energy. Further investigations are underway into the structure of these core–shell nanoparticles and their applicability.

METHODS

All operations were carried out under inert atmosphere in an argon-filled LC-Technology glovebox (<1 ppm O_2 and H_2O). All chemicals and dry solvents were purchased from Sigma-Aldrich.

Synthesis of $NaBH_4$ Nanoparticles. Nanoparticles of $NaBH_4$ were prepared by antisolvent precipitation. A saturated solution of $NaBH_4$ was prepared by dissolving 500 mg of $NaBH_4$ in 10 mL of dry diglyme at 50 °C. Then 0.5 g of tetra-*n*-butylammonium bromide (TBAB) was added to enhance solubility and act as a stabilizing agent. The solution of borohydride was then filtered to remove any undissolved compound and added dropwise to a 50 mL solution of dry pentane kept at 5 °C under fast magnetic stirring. The resulting precipitate was separated by centrifugation, washed in tetrahydrofuran (THF), and dried under vacuum at room temperature, leading to nanoparticles of $NaBH_4$ stabilized by TBAB at a concentration of 22 mass % as observed by TGA. The particles could be resuspended without aggregation, but sedimentation of suspensions occurred after several days.

Synthesis of the Core–shell Particles $NaBH_4$@Ni. As-synthesized $NaBH_4$ nanoparticles (100 mg) were suspended in 5 mL of THF. Fifty milligrams of anhydrous nickel(II) chloride was suspended in 5 mL of THF and added dropwise to the suspension of nanoparticles. The concentration of $NiCl_2$ added was based on an estimate of the amount required to react with only the surface borohydride ions. This was calculated based on the number of α-$NaBH_4$ unit cells assumed to be in an average $NaBH_4$ nanoparticle and was determined to be 0.038 mol·L^{-1} (see Supporting Information). Higher and lower concentrations of $NiCl_2$ (*i.e.*, 25 and 100 mg) were also tested for comparison, and the optimal amount of $NiCl_2$ was found to be 50 mg (Supporting Information Figure S10). After around 1 min, the suspension turned black and was allowed to age overnight before separation by centrifugation, washing three times with THF, and drying under vacuum at room temperature. According to elemental analysis, the resulting core–shell nanoparticles contained 42.6 ± 1.0 mass % Na, 16.5 ± 1.0 mass % Ni, 14.9 ± 1.0 mass % B, and 19.0 ± 1.1 mass % Cl. Assuming that $NiCl_2$ was fully reacted and all Cl was present in NaCl, this corresponds to a NaCl content of 31.3 ± 1.1% and a $NaBH_4$ content of 49.7 ± 1.0%, with an overall hydrogen capacity of 5.3 ± 1.0%. The remaining mass comprised nickel. We observed that the material was stable once exposed to air. However, the metallic nickel coating may oxidize.

Characterization. The nickel, sodium, and boron contents were determined by inductively coupled plasma optical emission spectroscopy (ICP-OES) with a Perkin-Elmer OPTIMA 7300 ICP-OES instrument. Chloride content was determined by anion chromatography using a Dionex ion chromatography system with autosampler. Prior to analysis, the material (~20 mg) was dissolved into 400 μL of concentrated nitric acid and diluted 20 times with high purity water.

The size, morphology, and EDS analysis and elemental mapping of the particles were characterized by transmission electron microscopy (TEM) using a Philips CM200 operated at 200 keV and scanning electron microscopy (SEM) using a FEI Nova NanoSEM 230 FESEM. TEM samples were dispersed in THF, sonicated for a few seconds, and then dropped onto a carbon-coated copper grid. Similarly desorbed and cycled samples were dispersed in THF and dropped onto a carbon-coated grid. SEM samples were dispersed on a carbon tape. Exposure to air was limited to transfer between an Ar-filled sample tube containing the materials to image and the instruments.

The crystalline nature of the materials synthesized was determined by X-ray diffraction (XRD) using a Philips X'pert Multipurpose XRD system operated at 40 mA and 45 kV with a monochromated Cu Kα radiation (λ = 1.541 Å): step size = 0.01, 0.02, or 0.05, time per step = 10 or 20 s/step. The materials were protected against oxidation from air by a Kapton foil. For Raman spectroscopy, the materials were placed in quartz capillaries sealed under the inert argon atmosphere of a glovebox. Raman spectra were collected with a Renishaw inVia Raman microscope with a 514 nm argon ion laser.

The chemical properties of the surface of the nanoparticles were characterized by X-ray photoelectron spectroscopy (XPS) using an ESCALAB250Xi from Thermo Scientific. The incident radiation was monochromatic A1 X-rays (1486.6 eV) at 164 W (15.2 kV, 10.8 ma) with a spot size of 500 μm. Survey (wide) scans were taken at analyzer pass energy of 100 eV and multiplex (narrow) higher resolution scans at 20 eV. Survey scans were carried out over 1200–0 eV binding energy range with 1.0 eV steps. Narrow higher resolution scans were run with 0.1 eV steps. Base pressure in the analysis chamber was 2.0×10^{-9} mbar. The data were analyzed using XPS Avantage software. Exposure to air of the samples was limited to transfer between an argon-filled sample tube and the instrument.

Thermogravimetric analysis (TGA) and differential scanning calorimetry (DSC) in conjunction with mass spectrometry (MS) were conducted at 10 °C·min^{-1} under an argon flow of 25 mL·min^{-1} using a Mettler Toledo TGA/DSC 1 coupled with an Omnistar MS. Masses between m/e = 2 and 99 were followed.

Hydrogen desorption/absorption kinetics were characterized with a high-pressure magnetic balance of 1 μg resolution equipped with capability for simultaneous density measurements (Rubotherm). The material was first cycled once at 150 and 250 °C to allow a gradual dehydrogenation of $NaBH_4$@Ni before cycling at 350 °C. Twenty milligrams of material was used with a hydrogen pressure of 4 MPa for absorption and 0.01 MPa for desorption. Hydrogen uptake and release were determined from the weight changes. For an accurate determination of the amount of hydrogen stored, a blank measurement with the empty sample holder was performed at 350 °C to determine the mass and volume of the sample holder. Further measurements were performed at 350 °C under a He atmosphere with the material fully desorbed to determine the density of the materials and corresponding parameters for buoyancy corrections. To enable further characterization of the cycled $NaBH_4$@Ni, larger amounts (~200 mg) of material were cycled on a manual volumetric system (Sievert type) under identical conditions of pressure and temperature.

Conflict of Interest: The authors declare no competing financial interest.

Acknowledgment. This research was supported by UNSW Internal Research Grant program and under the Australian Research Council's Discovery Projects funding scheme (project DP1095209). We appreciate the use of instruments in the Mark Wainwright Analytical Center at UNSW.

Supporting Information Available: Calculation of $NiCl_2$ content required. Additional SEM and TEM images of bulk $NaBH_4$, nano-$NaBH_4$, and $NaBH_4$@ Ni and associated particle size distributions. Thermal decomposition of TBAB and MS associated with the decomposition of TBAB in nano-$NaBH_4$. Second, third, and fourth hydrogen cycles for $NaBH_4$@Ni. XPS of $NaBH_4$@Ni, survey and narrow scan for Na1s and Cl2p and B1s. TGA/DSC of $NaBH_4$@Ni after hydrogen absorption. EDS mapping of $NaBH_4$@Ni after cycling. Effect of $NiCl_2$ content on hydrogen desorption from $NaBH_4$@Ni. This material is available free of charge *via* the Internet at http://pubs.acs.org.

REFERENCES AND NOTES

1. Motyka, T.; Zidan, R.; Summers, W. *Hydrogen Storage: The Key Challenge Facing a Hydrogen Economy*; United States Department of Energy, 2004.
2. Eberle, U.; Felderhoff, M.; Schüth, F. Chemical and Physical Solutions for Hydrogen Storage. *Angew. Chem., Int. Ed.* **2009**, *48*, 6608–6630.
3. Aguey-Zinsou, K.; Ares-Fernandez, J. Hydrogen in Magnesium: New Perspectives toward Functional Stores. *Energy Environ. Sci.* **2010**, *3*, 526–543.
4. Ren, R.; Ortiz, A. L.; Markmaitree, T.; Osborn, W.; Shaw, L. L. Stability of Lithium Hydride in Argon and Air. *J. Phys. Chem. B* **2006**, *110*, 10567–10575.
5. Jain, I. P.; Jain, P.; Jain, A. Novel Hydrogen Storage Materials: A Review of Lightweight Complex Hydrides. *J. Alloys Compd.* **2010**, *503*, 303–339.
6. Orimo, S.; Nakamori, Y.; Eliseo, J.; Züttel, A.; Jensen, C. Complex Hydrides for Hydrogen Storage. *Chem. Rev.* **2007**, *107*, 4111–4132.
7. Züttel, A.; Borgschulte, A.; Orimo, S.-I. Tetrahydroborates as New Hydrogen Storage Materials. *Scr. Mater.* **2007**, *56*, 823–828.
8. Ares, J. R.; Aguey-Zinsou, K. F.; Leardini, F.; Ferrer, I. J.; Fernandez, J. F.; Guo, Z. X.; Sanchez, C. Hydrogen Absorption/Desorption Mechanism in Potassium Alanate ($KAlH_4$) and Enhancement by $TiCl_3$ Doping. *J. Phys. Chem. C* **2009**, *113*, 6845–6851.
9. Roennebro, E.; Majzoub, E. H. Calcium Borohydride for Hydrogen Storage: Catalysis and Reversibility. *J. Phys. Chem. B* **2007**, *111*, 12045–12047.
10. Severa, G.; Ronnebro, E.; Jensen, C. M. Direct Hydrogenation of Magnesium Boride to Magnesium Borohydride: Demonstration of >11 Weight Percent Reversible Hydrogen Storage. *Chem. Commun.* **2010**, *46*, 421–423.
11. Ares, J. R.; Aguey-Zinsou, K. F.; Porcu, M.; Sykes, J. M.; Dornheim, A.; Klassen, T.; Bormann, R. Thermal and Mechanically Activated Decomposition of $LiAlH_4$. *Mater. Res. Bull.* **2008**, *43*, 1263–1275.

12. Li, H.-W.; Yan, Y.; Orimo, S.-I.; Züttel, A.; Jensen, C. M. Recent Progress in Metal Borohydrides for Hydrogen Storage. *Energies* **2011**, *4*, 185–214.
13. Bogdanovic, B.; Felderhoff, M.; Streukens, G. Hydrogen Storage in Complex Metal Hydrides. *J. Serb. Chem. Soc.* **2009**, *74*, 183–196.
14. Aguey-Zinsou, K.; Yao, J.; Guo, Z. Reaction Paths between $LiNH_2$ and LiH with Effects of Nitrides. *J. Phys. Chem. B* **2007**, *111*, 12531–12536.
15. Xiong, Z.; Yong, C.; Wu, G.; Chen, P.; Shaw, W.; Karkamkar, A.; Autrey, T.; Jones, M.; Johnson, S.; Edwards, P.; David, W. High-Capacity Hydrogen Storage in Lithium and Sodium Amidoboranes. *Nat. Mater.* **2008**, *7*, 138–141.
16. Nakamori, Y.; Orimo, S. Destabilization of Li-Based Complex Hydrides. *J. Alloys Compd.* **2004**, *370*, 271–275.
17. Pinkerton, F.; Meyer, M.; Meisner, G.; Balogh, M.; Vajo, J. Phase Boundaries and Reversibility of $LiBH_4/MgH_2$ Hydrogen Storage Material. *J. Phys. Chem. C* **2007**, *111*, 12881–12885.
18. Vajo, J.; Olson, G. Hydrogen Storage in Destabilized Chemical Systems. *Scr. Mater.* **2007**, *56*, 829–834.
19. Yu, X.; Guo, Y.; Sun, D.; Yang, Z.; Ranjbar, A.; Guo, Z.; Liu, H.; Dou, S. A Combined Hydrogen Storage System of $Mg(BH_4)_2-LiNH_2$ with Favorable Dehydrogenation. *J. Phys. Chem. C* **2010**, *114*, 4733–4737.
20. Bösenberg, U.; Kim, J. W.; Gosslar, D.; Eigen, N.; Jensen, T. R.; von Colbe, J. M. B.; Zhou, Y.; Dahms, M.; Kim, D. H.; Günther, R.; *et al.* Role of Additives in $LiBH_4-MgH_2$ Reactive Hydride Composites for Sorption Kinetics. *Acta Mater.* **2010**, *58*, 3381–3389.
21. Wellons, M.; Berseth, P.; Zidan, R. Novel Catalytic Effects of Fullerene for $LiBH_4$ Hydrogen Uptake and Release. *Nanotechnology* **2009**, *20*, 204022.
22. Fernandez, J. R. A.; Aguey-Zinsou, F.; Elsaesser, M.; Ma, X. Z.; Dornheim, M.; Bormann, R. Mechanical and Thermal Decomposition of $LiAlH_4$ with Metal Halides. *Int. J. Hydrogen Energy* **2007**, *32*, 1033–1040.
23. Baxter, J.; Bian, Z.; Chen, G.; Danielson, D.; Dresselhaus, M. S.; Fedorov, A. G.; Fisher, T. S.; Jones, C. W.; Maginn, E.; Kortshagen, U.; *et al.* Nanoscale Design To Enable the Revolution in Renewable Energy. *Energy Environ. Sci.* **2009**, *2*, 559–588.
24. Fichtner, M. Properties of Nanoscale Metal Hydrides. *Nanotechnology* **2009**, *20*, 204009.
25. Aguey-Zinsou, K.-F.; Ares-Fernandez, J.-R. Synthesis of Colloidal Magnesium: A Near Room Temperature Store for Hydrogen. *Chem. Mater.* **2008**, *20*, 376–378.
26. Nielsen, T. K.; Besenbacher, F.; Jensen, T. R. Nanoconfined Hydrides for Energy Storage. *Nanoscale* **2011**, *3*, 2086–2098.
27. Vajo, J. J. Influence of Nano-Confinement on the Thermodynamics and Dehydrogenation Kinetics of Metal Hydrides. *Curr. Opin. Solid State Mater. Sci.* **2011**, *15*, 52–61.
28. Nielsen, T. K.; Manickam, K.; Hirscher, M.; Besenbacher, F.; Jensen, T. R. Confinement of MgH_2 Nanoclusters within Nanoporous Aerogel Scaffold Materials. *ACS Nano* **2009**, *3*, 3521–3528.
29. Christian, M.; Aguey-Zinsou, K.-F. Destabilisation of Complex Hydrides through Size Effects. *Nanoscale* **2010**, *2*, 2587–2590.
30. Lohstroh, W.; Roth, A.; Hahn, H.; Fichtner, M. Thermodynamic Effects in Nanoscale $NaAlH_4$. *ChemPhysChem.* **2010**, *11*, 789–792.
31. Stephens, R.; Gross, A.; Van Atta, S.; Vajo, J.; Pinkerton, F. The Kinetic Enhancement of Hydrogen Cycling in $NaAlH_4$ by Melt Infusion into Nanoporous Carbon Aerogel. *Nanotechnology* **2009**, *20*, 204018.
32. Zheng, S.; Fang, F.; Zhou, G.; Chen, G.; Ouyang, L.; Zhu, M.; Sun, D. Hydrogen Storage Properties of Space-Confined $NaAlH_4$ Nanoparticles in Ordered Mesoporous Silica. *Chem. Mater.* **2008**, *20*, 3954–3958.
33. Cahen, S.; Eymery, J.; Janot, R.; Tarascon, J. Improvement of the $LiBH_4$ Hydrogen Desorption by Inclusion into Mesoporous Carbons. *J. Power Sources* **2009**, *189*, 902–908.
34. Fang, Z.; Wang, P.; Rufford, T.; Kang, X.; Lu, G.; Cheng, H. Kinetic- and Thermodynamic-Based Improvements of Lithium Borohydride Incorporated into Activated Carbon. *Acta Mater.* **2008**, *56*, 6257–6263.
35. Gross, A.; Vajo, J.; Van Atta, S.; Olson, G. Enhanced Hydrogen Storage Kinetics of $LiBH_4$ in Nanoporous Carbon Scaffolds. *J. Phys. Chem. C* **2008**, *112*, 5651–5657.
36. Ngene, P.; Adelhelm, P.; Beale, A.; de Jong, K.; de Jongh, P. $LiBH_4$/SBA-15 Nanocomposites Prepared by Melt Infiltration under Hydrogen Pressure: Synthesis and Hydrogen Sorption Properties. *J. Phys. Chem. C* **2010**, *114*, 6163–6168.
37. Wu, H.; Zhou, W.; Wang, K.; Udovic, T.; Rush, J.; Yildirim, T.; Bendersky, L.; Gross, A.; Van Atta, S.; Vajo, J.; *et al.* Size Effects on the Hydrogen Storage Properties of Nanoscaffolded $Li_3BN_2H_8$. *Nanotechnology* **2009**, *20*, 204002.
38. Ampoumogli, A.; Steriotis, T.; Trikalitis, P.; Giasafaki, D.; Bardaji, E. G.; Fichtner, M.; Charalambopoulou, G. Nanostructured Composites of Mesoporous Carbons and Boranates as Hydrogen Storage Materials. *J. Alloys Compd.* **2011**, *509*, S705–S708.
39. Ngene, P.; van den Berg, R.; Verkuijlen, M. H. W.; de Jong, K. P.; de Jongh, P. E. Reversibility of the Hydrogen Desorption from $NaBH_4$ by Confinement in Nanoporous Carbon. *Energy Environ. Sci.* **2011**, *4*, 4108–4115.
40. Mueller, T.; Ceder, G. Effect of Particle Size on Hydrogen Release from Sodium Alanate Nanoparticles. *ACS Nano* **2010**, *4*, 5647–5656.
41. Zhao-Karger, Z.; Hu, J.; Roth, A.; Wang, D.; Kuebel, C.; Lohstroh, W.; Fichtner, M. Altered Thermodynamic and Kinetic Properties of MgH_2 Infiltrated in Microporous Scaffold. *Chem. Commun.* **2010**, *46*, 8353–8355.
42. Rodriguez-Reinoso, F.; Molina-Sabio, M. Textural and Chemical Characterization of Microporous Carbons. *Adv. Colloid Interface Sci.* **1998**, *76*, 271–294.
43. Grochala, W.; Edwards, P. Thermal Decomposition of the Non-Interstitial Hydrides for the Storage and Production of Hydrogen. *Chem. Rev.* **2004**, *104*, 1283–1315.
44. Santos, D. M. F.; Sequeira, C. A. C. Sodium Borohydride as a Fuel for the Future. *Renewable Sustainable Energy Rev.* **2011**, *15*, 3980–4001.
45. Demirci, U. B.; Akdim, O.; Miele, P. Ten-Year Efforts and a No-Go Recommendation for Sodium Borohydride for On-Board Automotive Hydrogen Storage. *Int. J. Hydrogen Energy* **2009**, *34*, 2638–2645.
46. Mao, J. F.; Guo, Z. P.; Nevirkovets, I. P.; Liu, H. K.; Dou, S. X. Hydrogen De-/Absorption Improvement of $NaBH_4$ Catalyzed by Titanium-Based Additives. *J. Phys. Chem. C* **2012**, *116*, 1596–1604.
47. Orimo, S.; Nakamori, Y.; Zuttel, A. Material Properties of MBH_4 (M = Li, Na, and K). *Mater. Sci. Eng. B* **2004**, *108*, 51–53.
48. Cushing, B. L.; Kolesnichenko, V. L.; O'Connor, C. J. Recent Advances in the Liquid-Phase Syntheses of Inorganic Nanoparticles. *Chem. Rev.* **2004**, *104*, 3893–3946.
49. Urgnani, J.; Torres, F. J.; Palumbo, M.; Baricco, M. Hydrogen Release from Solid State $NaBH_4$. *Int. J. Hydrogen Energy* **2008**, *33*, 3111–3115.
50. Stasinevich, D. S.; Egorenko, G. A. Thermographic Investigation of Alkali Metal and Magnesium Tetrahydroborates at Pressures up to 10 atm. *Russ. J. Inorg. Chem.* **1968**, *13*, 341–343.
51. *CRC Handbook of Chemistry and Physics*, 92nd ed.; CRC Press: Boca Raton, FL, 2012.
52. Martelli, P.; Caputo, R.; Remhof, A.; Mauron, P.; Borgschulte, A.; Züttel, A. Stability and Decomposition of $NaBH_4$. *J. Phys. Chem. C* **2010**, *114*, 7173–7177.
53. Pendolino, F.; Mauron, P.; Borgschulte, A.; Züttel, A. Effect of Boron on the Activation Energy of the Decomposition of $LiBH_4$. *J. Phys. Chem. C* **2009**, *113*, 17231–17234.
54. James, B. D.; Wallbridge, M. G. H. Metal Tetrahydroborates. In *Progress in Inorganic Chemistry*; Lippard, S. J., Ed.; John Wiley & Sons: Hoboken, NJ, 2007; pp 209–210.
55. Ngene, P.; Verkuijlen, M. H. W.; Zheng, Q.; Kragten, J.; van Bentum, P. J. M.; Bitter, J. H.; de Jongh, P. E. The Role of Ni in Increasing the Reversibility of the Hydrogen Release from Nanoconfined $LiBH_4$. *Faraday Discuss.* **2011**, *151*, 47–58.

56. Liu, J.; Qiao, S. Z.; Chen, J. S.; Lou, X. W.; Xing, X.; Lu, G. Q. Yolk/Shell Nanoparticles: New Platforms for Nanoreactors, Drug Delivery and Lithium-Ion Batteries. *Chem. Commun.* **2011**, *47*, 12578–12591.
57. Chaudhuri, R. G.; Paria, S. Core/Shell Nanoparticles: Classes, Properties, Synthesis Mechanisms, Characterization, and Applications. *Chem. Rev.* **2012**, *112*, 2373–2433.
58. Glavee, G. N.; Klabunde, K. J.; Sorensen, C. M.; Hadjipanayis, G. C. Borohydride Reduction of Nickel and Copper Ions in Aqueous and Nonaqueous Media. Controllable Chemistry Leading to Nanoscale Metal and Metal Boride Particles. *Langmuir* **1994**, *10*, 4726–4730.
59. Tsyganov, S.; Kaestner, J.; Rellinghaus, B.; Kauffeldt, T.; Westerhoff, F.; Wolf, D. Analysis of Ni Nanoparticle Gas Phase Sintering. *Phys. Rev. B* **2007**, *75*, 045421.
60. Matsumo, M.; Bionifacio, C. S.; Thron, A. M.; Rufner, J.; Holland, T. B.; van Bethem, K. *In Situ* Sintering of Ni Nanoparticles by Controlled Heating. *Microsc. Microanal.* **2011**, *17*, 524–525.
61. Reed, D.; Book, D. Recent Applications of Raman Spectroscopy to the Study of Complex Hydrides for Hydrogen Storage. *Curr. Opin. Solid State Mater. Sci.* **2010**, *15*, 62–72.
62. Kumar, M. P. S.; Viswanathan, B.; Swamy, C. S.; Srinivasan, V. Surface Properties of $CaNi_5$ Hydrogen Storage Alloy. *J. Mater. Sci.* **1989**, *24*, 4387–4391.
63. Renaudin, G.; Gomes, S.; Hagemann, H.; Keller, L.; Yvon, K. Structural and Spectroscopic Studies on the Alkali Borohydrides MBH_4 (M = Na, K, Rb, Cs). *J. Alloys Compd.* **2004**, *375*, 98–106.
64. Hashimoto, S.; Tsuda, T.; Ogata, K.; Sugahara, T.; Inoue, Y.; Ohgaki, K. Thermodynamic Properties of Hydrogen + Tetra-*n*-butylammonium Bromide Semi-Clathrate Hydrate. *J. Thermyn.* **2010**, 170819.